

Electronic Supplementary Information

Magnetic orientation behavior of L-type zeolite with rare-earth elements under low magnetic field

Tomomi Tabata,^a Anna Nagai^b and Motohide Matsuda ^{*b}

- ^a. *Department of Materials Science and Engineering, Graduate School of Science and Technology, Kumamoto University, 2-39-1 Kurokami, Chuo-ku, Kumamoto 860-8555, Japan.*
- ^b. *Faculty of Advanced Science and Technology, Kumamoto University, 2-39-1 Kurokami, Chuo-ku, Kumamoto 860-8555, Japan.*
E-mail: mm_2008@alpha.msre.kumamoto-u.ac.jp (Motohide Matsuda)

Table S1 Ion-exchange rate of L-type zeolite ion-exchanged with various rare-earth ions.

Zeolite	Ion-exchange rate / %
Ce-L	19
Pr-L	20
Nd-L	21
Eu-L	25
Tb-L	22
Dy-L	22
Tm-L	22
Yb-L	20

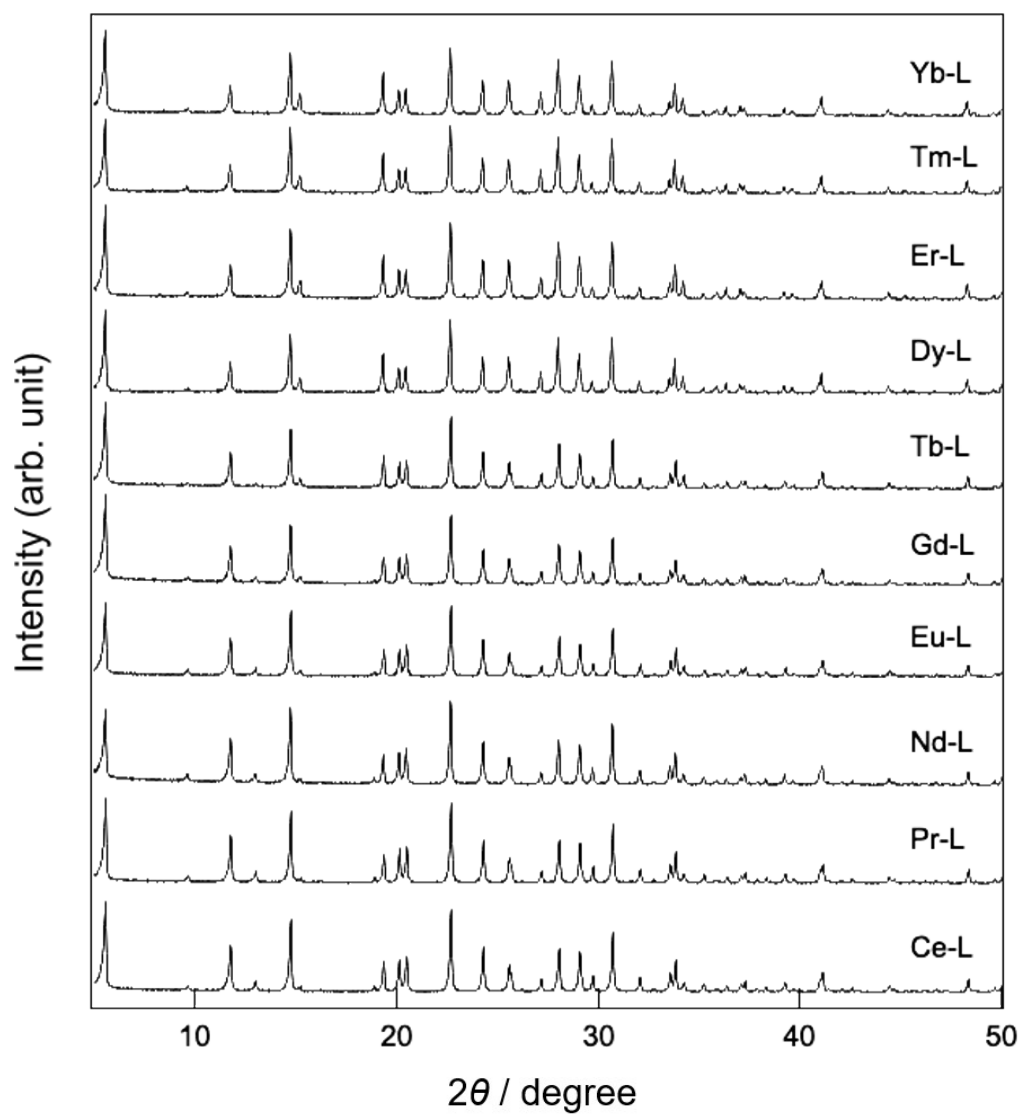


Figure S1 XRD patterns of L-type zeolite ion-exchanged with various rare-earth ions.

Table S2 Chemical compositions of K-L, Ho-L and K'-L powders.

	Components / mass%				
	O	Al	Si	K	Ho
K-L	50.2	9.1	27.2	13.5	
Ho-L	50.3	8.9	26.1	9.7	5.0
K'-L	49.6	9.2	27.1	13.1	1.0

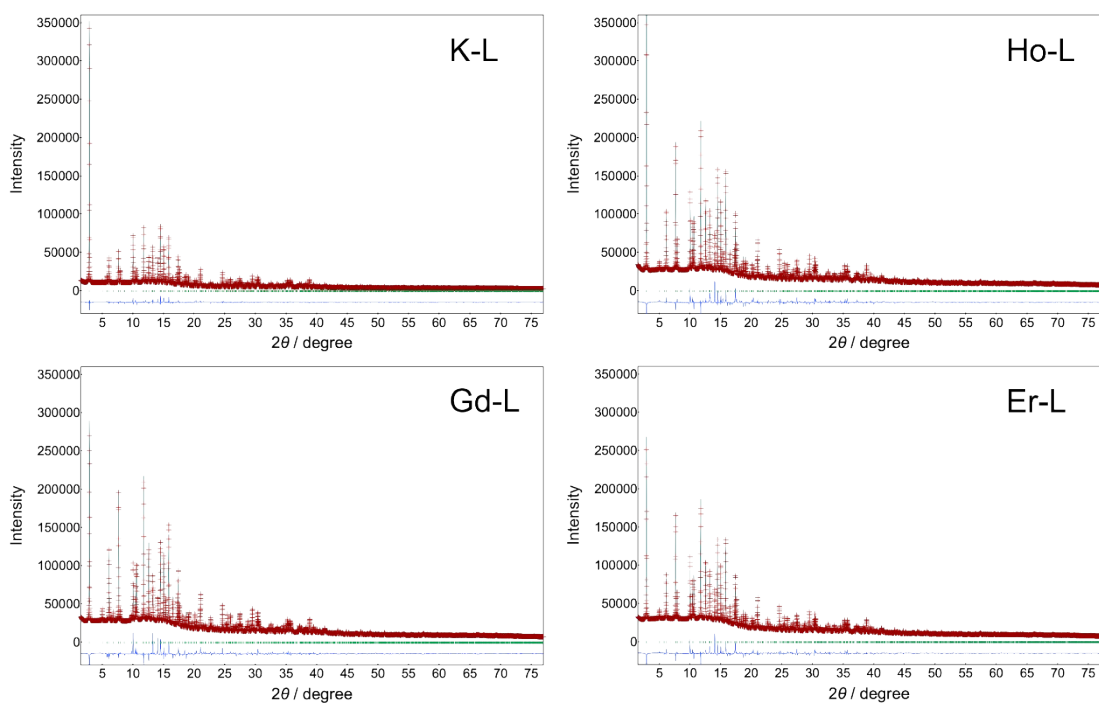


Figure S2 Rietveld refinement patterns for the synchrotron X-ray powder diffraction data. Observed diffraction intensities are represented by +, and the calculated pattern by a solid line. Differences between the observed and calculated intensities are given at the bottom. Short vertical marks below the observed and calculated patterns indicate the positions of allowed Bragg reflections.

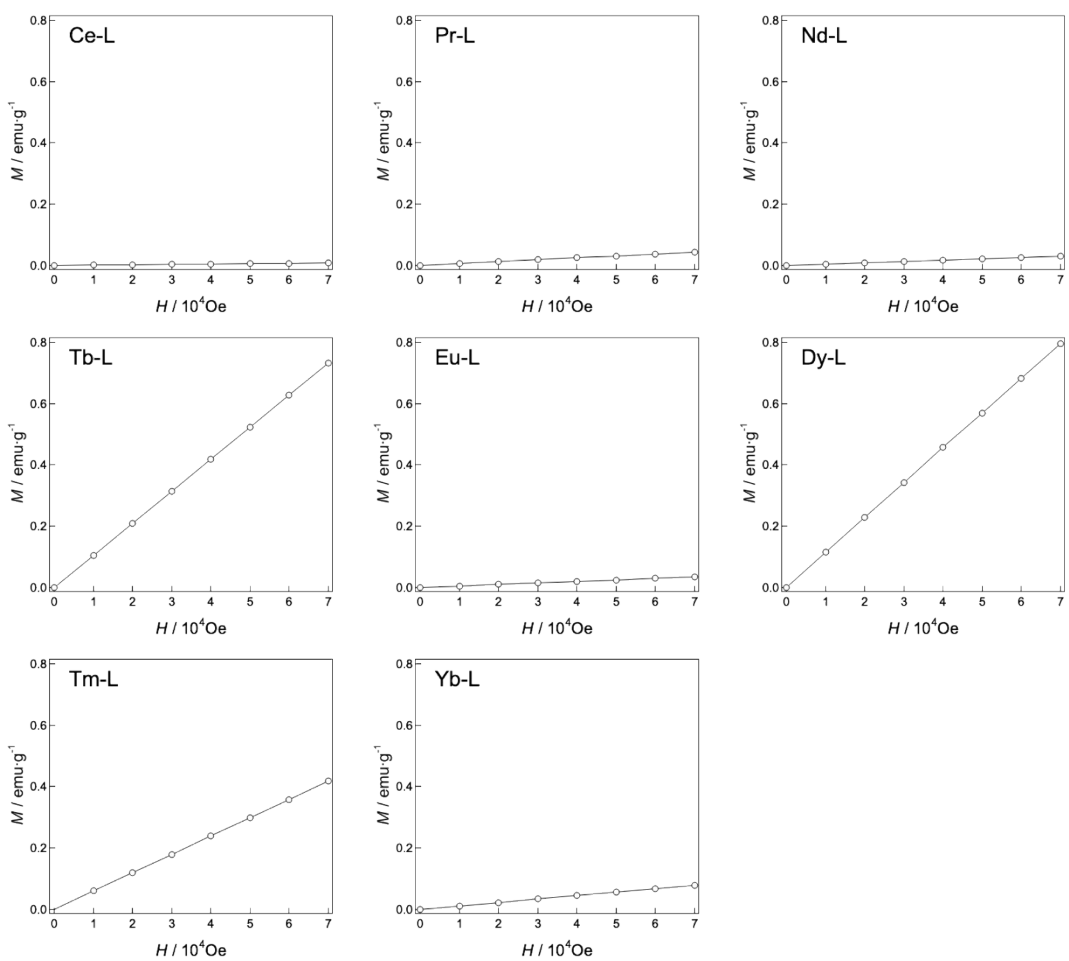


Figure S3 M - H curves of L-type zeolite ion-exchanged with various rare-earth ions.

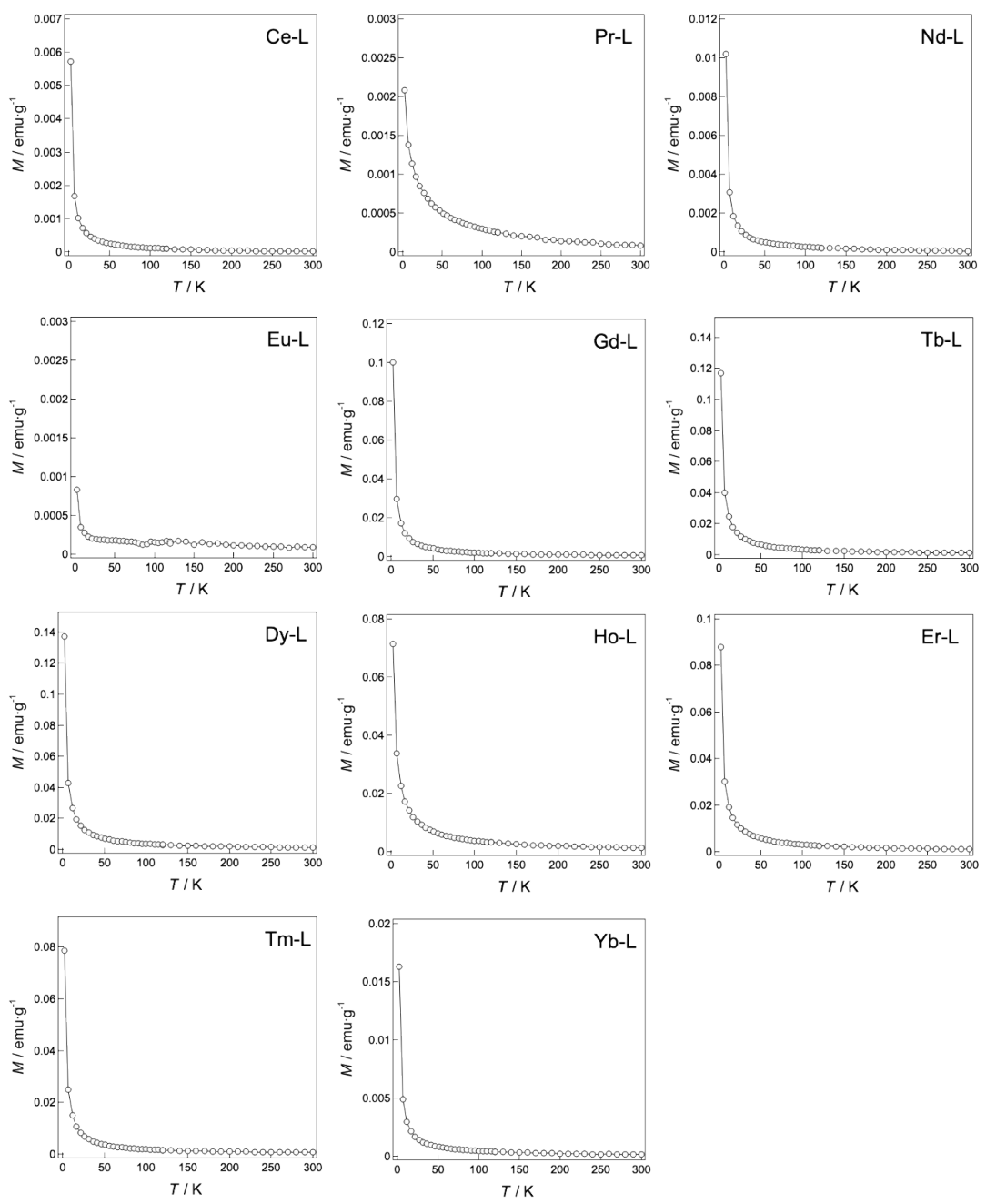


Figure S4 M - T curves of L-type zeolite ion-exchanged with various rare-earth ions.

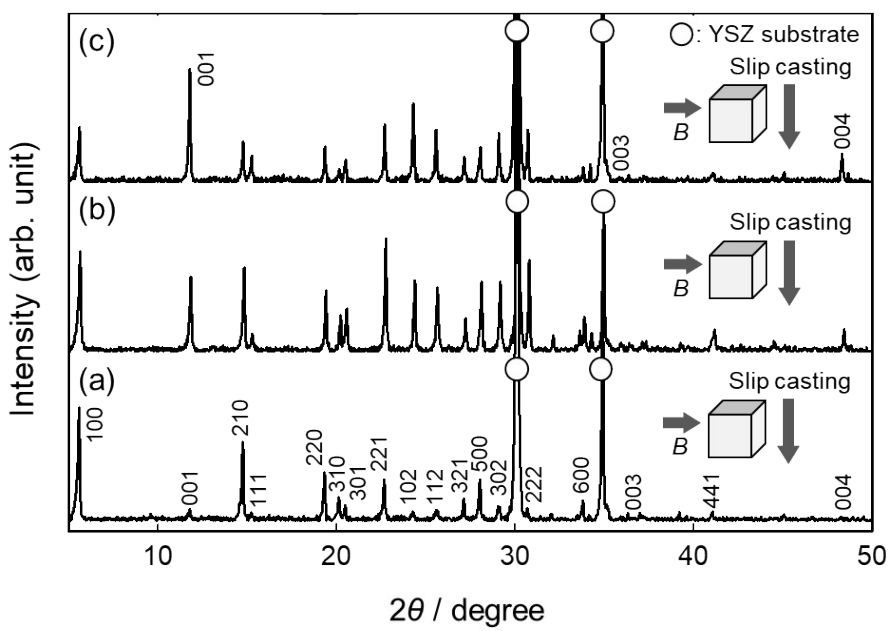


Figure S5 XRD patterns of powder-compacted films prepared with a 0.9 T magnetic field applied horizontally to the substrate surface for (a) Ho-L, (b) Gd-L and (c) Er-L, respectively.

Table S7 Interplanar angles, ϕ , between each lattice plane giving the characteristic peaks in powder XRD pattern and the (00l) planes estimated using the following equation given for a hexagonal cell ^{S1}:

$$\cos\phi = \frac{h_1 h_2 + k_1 k_2 + \frac{1}{2}(h_1 k_2 + h_2 k_1) + \frac{3}{4}\left(\frac{a}{c}\right)^2 l_1 l_2}{\sqrt{\left(h_1^2 + k_1^2 + h_1 k_1 + \frac{3}{4}\left(\frac{a}{c}\right)^2 l_1^2\right)\left(h_2^2 + k_2^2 + h_2 k_2 + \frac{3}{4}\left(\frac{a}{c}\right)^2 l_2^2\right)}}$$

$h \ k \ l$	$\phi / {}^\circ$
1 0 0	90
0 0 1	0
2 1 0	90
1 1 1	39.26
2 2 0	90
3 1 0	90
3 0 1	54.77
2 2 1	58.55
0 0 2	0
3 1 1	59.56
1 0 2	13.28
1 1 2	22.23
2 0 2	25.26
3 2 1	64.07
5 0 0	90
3 0 2	35.29
2 2 2	39.26
6 0 0	90
0 0 3	0
4 4 1	72.99
0 0 4	0

S1 B. D. Cullity, Element of X-ray Diffraction, second ed., Addison-Wesley Publishing Company, 1978 (Appendix C-3).

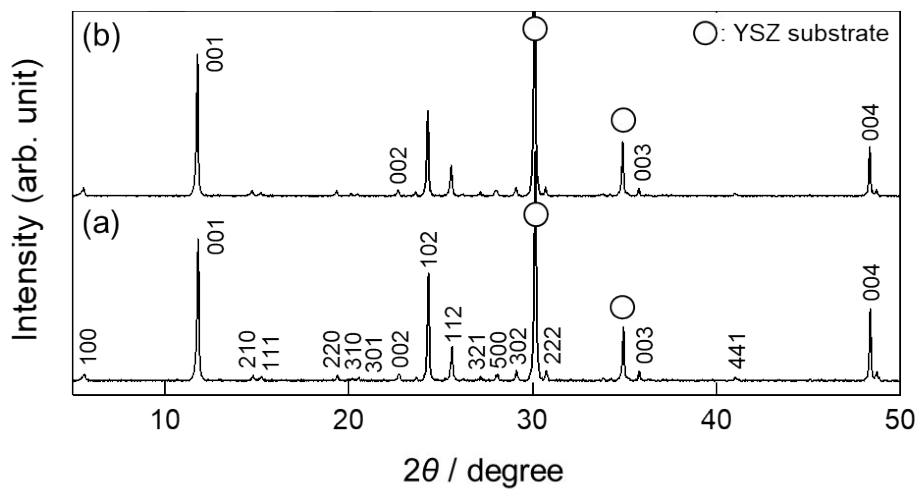


Figure S6 XRD patterns of Ho-compacted films with preferential orientation of the c-axis (a) before and (b) after reverse ion-exchange from Ho^{3+} to K^+ .

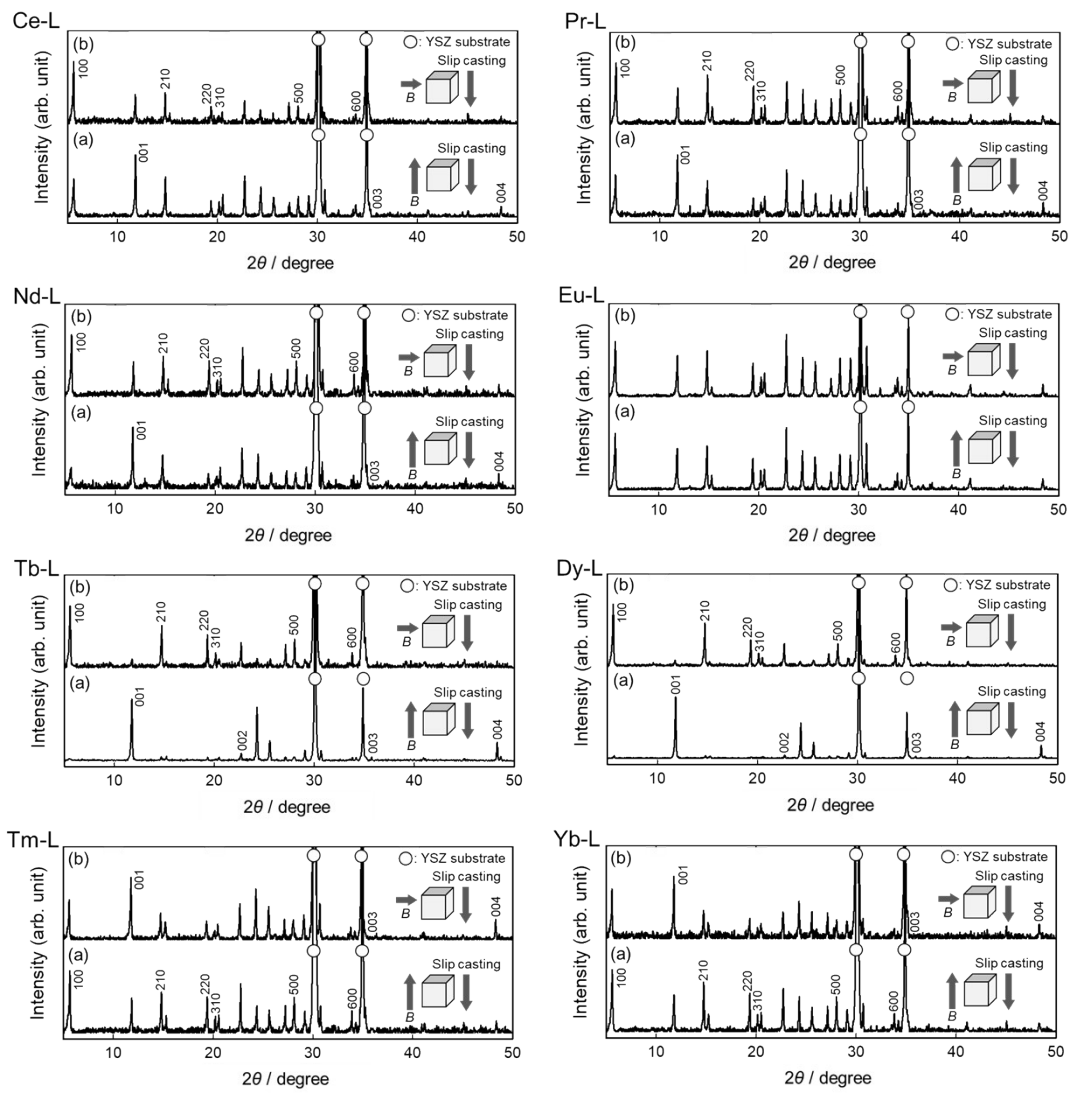


Figure S7 XRD patterns of the top of Ln (Ln = Ce, Pr, Nd, Eu, Tb, Dy, Tm and Yb)-compacted films prepared with a magnetic field (a) vertically and (b) horizontally applied to the substrate surface in the slip casting.

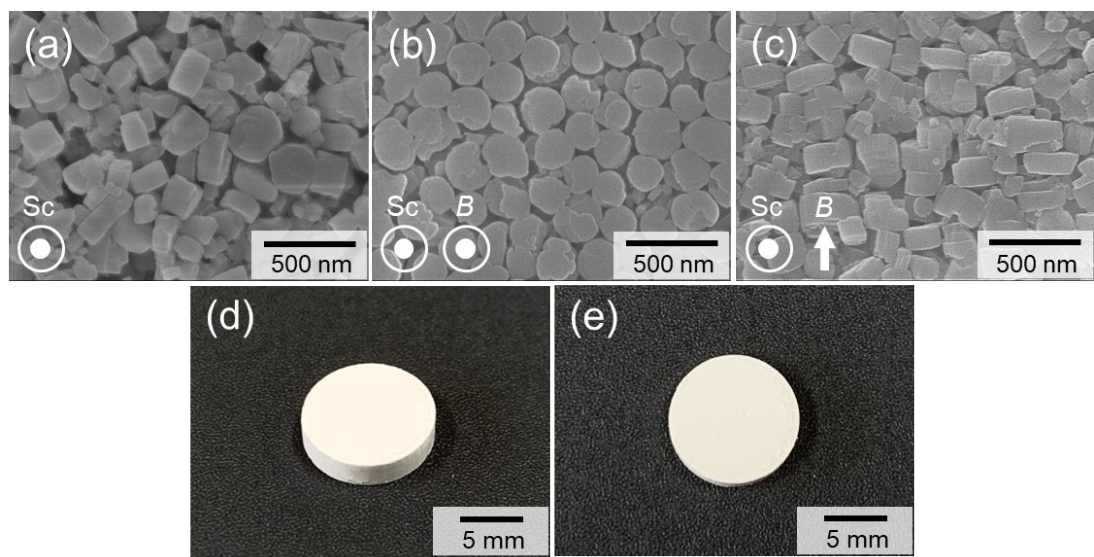


Figure S8 Surface SEM images for powder-compacted films of (a) random orientation, (b) the c -axis orientation and (c) the ab -plane orientation. The symbol of Sc in the SEM images indicates the direction of slip casting. Two photographs (d) and (e) are for the sample with the SEM image (b) in which the powder-compacted film is on a support substrate composed of an yttria-stabilized zirconia.